Effects of buffer layer thickness on the surface roughness of $In_{0.3}Ga_{0.7}As$ thin films: A phase-field simulation

Pingping Wu, Fangliang Gao, and Guoqiang Li[a)]
State Key Laboratory of Luminescent Materials and Devices, South China University of Technology, Guangzhou 510641, China

(Received 27 June 2013; accepted 4 October 2013)

The graded composition buffer layers are very commonly used in the semiconductor triple-junction solar cell device. To grow a strain-free 1.0-eV $In_{0.3}Ga_{0.7}As$ thin film on a GaAs substrate, a total of 2.2% misfit strain must be relaxed through well-designed buffer layer structures. In this work, a phase-field model of a multilayered system is developed to probe the roughness of top surface morphology and predict optimal buffer layer thickness. Our simulation shows time evolution of the thin film morphology and the root-mean-square roughness of the surface with different buffer layer thickness designs. The strain distribution is investigated to explain the surface morphology evolution with the effect of the buffer layer. The simulation results show that the buffer layer thickness is a key parameter that affects the quality of the $In_{0.3}Ga_{0.7}As$ epilayers. The simulation results can be effective in improving the design of graded buffer layers.

I. INTRODUCTION

In recent years, multijunction III–V solar cells have attracted increasing attention due to their very high conversion efficiency, and they generate many potential applications as a truly clean source of energy. The efficiencies can reach higher than 40% by triple-junction solar cell approaches.[1–4] The multilayered metamorphic or lattice mismatched epitaxial semiconductor system is usually used in a multijunction solar cell design. The key for the improvement of the material quality of the multilayered semiconductor thin film is the strain relaxation during the thin film growth process. In the strained multilayered heterostructure, threading dislocations or other defects generated by the strain relaxation can influence on the quality of the thin film. The compositional step graded buffer layers, as a very frequently used relaxation technology, can decrease the density of threading dislocations caused by the strain relaxation. The buffer structure introduces graded interfaces for the edge dislocations lying in the interface plane with the Burger's vector in the x–y direction[5]; therefore, it provides a high quality layer with a new lattice constant for the rest of the subcells to be grown on. In addition, buffer thickness has some relationships with the surface morphology and its root-mean-square (RMS) roughness. The buffer thickness has been proved to be an important factor of high quality thin films in many experimental works.[6–8] Wang et al.'s[7] SEM and optical measurement shows that a best surface morphology and lowest RMS roughness is achieved with a 20-nm buffer layer. Luo et al.'s[8] work shows that there is a significant decrease of RMS roughness during the initial stage of increasing buffer layer thickness. On the other hand, the surface morphology of the buffer layer has strong influence on the thin film quality. Nakamura[9] shows that the optimum thickness of the buffer layer is around 20 nm, thicker or thinner buffer layer can reduce the quality of the epitaxial thin film. Gonzalez et al.[10] demonstrate that the surface morphology of the buffer layer affects the surface of the thin film and the photovoltaic properties. Piquette et al.[11] observed that the surface morphology of the thin film is strongly dependent on the conditions of buffer layer deposition. In the crystal growth process, a buffer layer structure design has two main advantages: (i) avoid the high misfit strain between the top thin film and the substrate and (ii) decrease the defect density induced by the misfit strain, including both edge/screw dislocations and point defects. However, to fundamentally understand the physical mechanism in the buffer layers, the strain distribution in the step graded multilayers and its influence on the surface roughness are required. Thus, the optimized thickness for buffer layers can be predicted based on theoretical studies, but only few studies are done on the mesoscopic simulations.

In thermodynamics and kinetics theory, the stress-driven surface of a thin film grown on a substrate shows instabilities, which have been analyzed by Asaro and Tiller,[12] and Grinfeld[13] (ATG). The formation of surface undulations led to an increase in surface energy but reduced the elastic energy in the stressed thin film. The ATG theory, as a linear theory, is able to predict the critical wave length[14,15] for surface undulations or critical island size[16]

[a)]Address all correspondence to this author.
e-mail: msgli@scut.edu.cn
DOI: 10.1557/jmr.2013.320

for the nanodot structure. The critical wave length/island size plays an important role in the surface morphology evolution of a thin film. Recently, further theoretical development of the critical wave length/island size was developed by Krishnamurthy and Srolovitz,[17] and Liu and Lu[18,19] The ATG theory also can be investigated for the case of solid/solid interfaces (e.g., thin film/buffer layer interface) and the island formation process during the thin film growth.[20,21] However, it does not provide information on the surface morphology evolution, strain distribution evolution, and the detailed interactions between them.

Phase-field models have been proved to be a powerful tool to simulate self-assembled quantum dots and thin film structures.[22–25] In the previous studies, the phase-field method is proposed to investigate the stress-induced surface instabilities, the surface morphologies, the elastic strain/stress distributions, and the spontaneous formation mechanisms during the heteroepitaxial growth process. In this work, we used the phase-field method to simulate a multilayered heterostructure of a 1-eV junction as a bottom junction in the solar cell system. The 1-eV junction is theoretically predicted to be an optimal option for increasing the triple-junction solar cell efficiency.[26,27] We chose $In_{0.3}Ga_{0.7}As$ thin film grown on the GaAs substrate to be the 1-eV junction,[28] with a relatively large lattice misfit strain of ~2%.[29,30] Such a large misfit strain will induce nonideal growth due to the alloy layer relaxation by introduction of high dislocation density or the formation of three-dimensional islands.[31,32] To relax the misfit strain in $In_{0.3}Ga_{0.7}As$ thin film on the GaAs substrate, an $In_{0.15}Ga_{0.85}As$ buffer layer is introduced as a buffer layer. Therefore, our current work focuses on the investigation of the top surface roughness with multilayered heterostructures. The main purpose of this current paper is to explore the interplay between the buffer layers and the surface morphology through the strain distribution and revealing the effect of the thickness on the surface morphologies and roughness. In particular, the optimum buffer thickness based on our current phase-field model for the best surface quality is discussed. The strain distribution and the RMS roughness of the thin film surface are studied by addition of a buffer layer with its thickness ranged from 1 to 12 nm. The simulation results help us better understand the intrinsic mechanism of the strain relaxation by the multilayered thin film structures and improve the thin film quality with optimized buffer layer thickness.

II. SIMULATION METHOD

In this letter, we present a phase-field model taking into account the effect of the buffer layer between the thin film and the substrate. Figure 1 illustrates a schematic model of the system: to grow an $In_{0.3}Ga_{0.7}As$ thin film on the GaAs (001) substrate, a buffer layer of $In_{0.15}Ga_{0.85}As$ is introduced into the thin film/substrate interface. In this model, we used four conserved order parameters η_1, η_2, η_3, and η_4 to describe the volume fractions of the gas phase, $In_{0.3}Ga_{0.7}As$ thin film, (001) GaAs substrate, and the $In_{0.15}Ga_{0.85}As$ buffer layer. The total volume fraction of the system is fixed, i.e., $\eta_1 + \eta_2 + \eta_3 + \eta_4 = 1$.

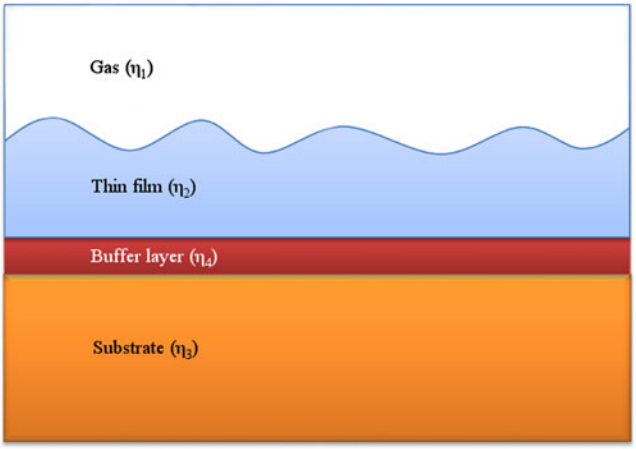

FIG. 1. The schematic of a thin film deposited on the substrate with a buffer layer structure.

For a conserved system, the temporal evolution of the surface morphology of the $In_{0.3}Ga_{0.7}As$ thin film is governed by nonlinear Cahn–Hilliard equations. As we assume the substrate phase (η_3) is static for simplicity, both the order parameters of the thin film (η_2) and the buffer layer (η_4) are chosen as independent phase field; thus the kinetic equations are:

$$\frac{\partial \eta_2}{\partial t} = \nabla\left[M\nabla\left(\frac{\delta F_{\text{tot}}}{\delta \eta_2}\right)\right] \quad , \tag{1}$$

$$\frac{\partial \eta_4}{\partial t} = \nabla\left[M\nabla\left(\frac{\delta F_{\text{tot}}}{\delta \eta_4}\right)\right] \quad , \tag{2}$$

where M is the phase-field mobility, t is the time, F_{tot} is the total free energy of the multiphase system, including bulk chemical energy (F_{chem}), surface/interface energy (F_{inter}), and elastic energy (F_{elas}). In our current model, we assume that mobility is a constant and neglect the difference between the bulk and surface diffusivities. The C–H equation describes the dynamics controlled by bulk diffusion. For simplicity, the value of mobility M is assumed to be the same for the thin film and the buffer layer.

The total free energy can be expressed by

$$F_{\text{tot}} = F_{\text{chem}} + F_{\text{inter}} + F_{\text{elas}} \quad . \tag{3}$$

The Landau-type coarse-grained bulk chemical free energy is

$$F_{\text{chem}} = \int -\left[\sum_{i\neq j} \omega_{ij}\eta_i^2\eta_j^2\right] \mathrm{d}V \quad i, j = 1, 2, 3, 4 \quad , \tag{4}$$

where ω_{ij} is the height of the double well potential, V is the total volume of the system.

The interface between order parameters η_i and η_j is denoted as γ_{ij}. For a four-order-parameter system, there are six possible interfaces: γ_{12}, γ_{13}, γ_{14}, γ_{23}, γ_{24}, and γ_{34}. The interfacial energy between the order parameters in the system can be written as

$$F_{\text{inter}} = \int -\sum_{i\neq j} \alpha_{ij}^2 \nabla\eta_i \cdot \nabla\eta_j \mathrm{d}V \quad i, j = 1, 2, 3, 4 \quad , \tag{5}$$

where α_{ij} is the gradient energy coefficient. The elastic energy of the thin film at a given strain state is calculated by using Khachaturyan's[33] microelastic theory:

$$F_{\text{elas}} = \frac{1}{2}\int \left[C_{ijkl}\left(\varepsilon_{ij} - \varepsilon_{ij}^0\right)\left(\varepsilon_{kl} - \varepsilon_{kl}^0\right)\right] \mathrm{d}V \quad , \tag{6}$$

where C_{ijkl} is the second order elastic tensor, the ε_{ij} is the total strain in the microelastic theory, and ε_{ij}^0 is the eigenstrain of the material,

$$\varepsilon_{ij}^0 = \sum_{p=1}^{3} \eta_p(\bar{r})\varepsilon_{ij}^{0,\eta_p} \quad , \tag{7}$$

where $\bar{r}$ is the coordinate. The final total free energy is calculated as the sum of the elastic energy, chemical energy, and the interface energy by Eq. (3). Equations (1) and (2) can be simultaneously solved by the semiimplicit Fourier-spectral method.[34]

III. RESULTS AND DISCUSSION

In the simulations, by considering a one-dimensional stationary equilibrium problem of the phase-field parameter, the gradient energy coefficients and the chemical energy parameters can be determined as

$$\alpha_{ij} = \sqrt{\frac{6\delta\beta_{ij}}{b}} \text{ and } \omega_{ij} = \frac{6\beta_{ij}b}{\delta} \quad , \tag{8}$$

where δ is the interface thickness, β_{ij} is the surface or interface energy between phases i and j, and b is a constant. The interface thickness is chosen to be $5\Delta x$, the surface energies for the InGaAs/GaAs system are $\beta_{12} = \beta_{13} = \beta_{14} = 0.5$ N/m, and the interfacial energies are $\beta_{23} = \beta_{24} = \beta_{34} = 0.26$ N/m.[35,36] b is chosen to be 2.2, for simplicity, we chose β as the average of β_{ij}, i.e., $\beta = 0.38$ N/m; thus the calculated height of the double well potential $\omega_{ij} = 1.0 \times 10^9$ N/m^2, and the gradient energy coefficient is $\alpha_{ij} = 7.2 \times 10^{-5}$ N$^{1/2}$. The elastic coefficients given in Ref. 37 are used here: for GaAs substrate: $C_{11} = 11.879 \times 10^{11}$ N/m^2, $C_{12} = 5.376 \times 10^{11}$ N/m^2, and $C_{44} = 5.94 \times 10^{11}$ N/m^2; for $In_{0.15}Ga_{0.85}As$ buffer layer: $C_{11} = 11.345 \times 10^{11}$ N/m^2, $C_{12} = 5.2485 \times 10^{11}$ N/m^2, and $C_{44} = 5.6415 \times 10^{11}$ N/m^2; for $In_{0.3}Ga_{0.7}As$ thin film: $C_{11} = 10.811 \times 10^{11}$ N/m^2, $C_{12} = 5.121 \times 10^{11}$ N/m^2, and $C_{44} = 5.343 \times 10^{11}$ N/m^2. The pseudocubic lattice parameters for GaAs, $In_{0.15}Ga_{0.85}As$, and $In_{0.3}Ga_{0.7}As$ at room temperature are set to be 5.6419, 5.70436, and 5.76682, respectively.[37,38] The mobility M is chosen to be 1.0×10^{-27} m^5/(J s). $256\Delta x_1 \times 64\Delta x_2$ discrete grid points are employed in this work with periodic boundary conditions applied along x_1 axes, where $\Delta x_1 = \Delta x_2 = 1.0$ nm. All the calculations are taken by 5000 time steps with a time step for integration of $\Delta t = 0.1$. The initial surface morphology is described by the thin film thickness $h(x)$, which is assumed to be a simple, static sinusoidal plane wave

$$h(x) = h_0 + \beta\sin(kx + \varphi) \quad , \tag{9}$$

where h_0 is the initial average thin film thickness, β is the amplitude, k is the wave number, and ϕ is the initial phase.

To describe the surface roughness of a solid thin film, the most common statistic used is the RMS roughness, which is defined as[39]

$$\text{RMS} = \sqrt{\langle[h(x) - \bar{h}]^2\rangle} \quad , \tag{10}$$

where $<\ldots>$ represents the average value of $\ldots$, and $\bar{h}$ is the mean height of the thin film surface. In the phase-field model, we suggest the distance between the point where $\eta_1 = \eta_2 = 0.5$ and $\eta_4 = \eta_3 = 0.5$ as the height of the surface.

As our current simulations did not include any defect mechanism, the thickness of the thin film and buffer layer must be below the critical thickness. According to the well known work of Matthews and Blakeslee's (M&B's) theory,[40] the critical thickness of the $In_xGa_{1-x}As$ expitaxial thin film can be written as[41]

$$h_c = \frac{4}{\pi\varepsilon_{\text{mf}}}\frac{(1 - \nu/4)}{(1 + \nu)}\left(\ln\frac{h_c}{4} + 1\right) \quad . \tag{11}$$

where h_c is the critical thickness, ν is the poission ratio, ε_{mf} is the misfit strain between the thin film and substrate which can be defined as

$$\varepsilon_{\text{mf}} = (a_f - a_s)/a_s \quad , \tag{12}$$

where a_f and a_s are the lattice parameters of the thin film and the substrate, respectively. For the GaAs/InGaAs

system, ν is chosen to be 0.312.[42,43] For an $In_{0.15}Ga_{0.85}As$ thin film as the buffer layer grown on the GaAs substrate, the misfit strain between the buffer layer and the substrate $\varepsilon_{mf} = 0.011$, the critical thickness by M&B's theoretical prediction is around 470 Å. For an $In_{0.3}Ga_{0.7}As$ thin film grown on the buffer layer, as we assumed that the $In_{0.3}Ga_{0.7}As$ thin film is under fully commensurate constraint and the buffer layer is coherently trained to have the same lattice constant as the substrate, the misfit strain between the thin film and the buffer layer is calculated by $\varepsilon_{mf} = (a_f - a_b)/a_b = (a_f - a_s)/a_s = 0.022$, where a_b is the lattice parameter for the buffer layer $In_{0.15}Ga_{0.85}As$, which implies the critical thickness of the top thin film is around 200 Å. Thus, the system with a total thickness under 670 Å (i.e., 67 nm) can be assumed to be defect free. The critical thickness measured in experimental works is somehow smaller than theoretical predictions. The experimental results in Refs. 44–46 show that the critical thickness of the $In_{0.15}Ga_{0.85}As$ monolayer thin film will not exceed 15 nm. In our simulations, we used 12 nm maximum for the $In_{0.15}Ga_{0.85}As$ buffer layer and an average thickness of 10 nm for the $In_{0.3}Ga_{0.7}As$ thin film, then the total thickness of the heterostructure is far below the critical thickness.

The simulated sequence of surface morphology evolution of the multiphase system is shown in Figures 2(a)–2(d). The initial profile of a sinusoidal wave surface morphology is used with the average thin film thickness $h_0 = 10$ nm and the amplitude $\beta = 5$ nm. The thickness of the buffer layer is assumed to be 5 nm. Figure 2(a) plots the prepared initial morphology of the thin film surface. Figures 2(b)–2(d) describes the thin film surface with the buffer layer at a time step of 1000, 3000, and 5000, respectively. It is clearly demonstrated that the surface morphology continues to smooth out from the initial profile with an $In_{0.15}Ga_{0.85}As$ buffer layer. The sinusoidal-wave-shaped surface morphology can still be seen in the initial 1000 steps, as shown in Fig. 2(b). It can be seen that the amplitude of the sinusoidal wave continues to decrease and the surface smoothes out to relax the internal strain. Finally, only several small fluctuations are observed.

To better understand the details of the strain relaxation mechanism with the buffer layer, the strain distributions at $t^* = 1000$ and $t^* = 5000$ are shown in Figs. 2(e) and 2(f). For initial sinusoidal-wave-shaped morphology, it can be seen that the strain becomes more compressive at the bottom of the wave but even tensile on the top of the wave, which is similar to the previous simulation results of nanodot coarsening.[21] Also, we note that the compressive strain is relaxed in the buffer layer, which proved the influence of the graded buffer. As there exists a buffer layer, a smooth surface morphology is favorable than nanodot shaped structures due to the strain relaxation in the buffer structure. The relaxation is confirmed by the strain distributions shown in Fig. 2(f). An average strain of around −0.011 is observed both in the thin film layer and

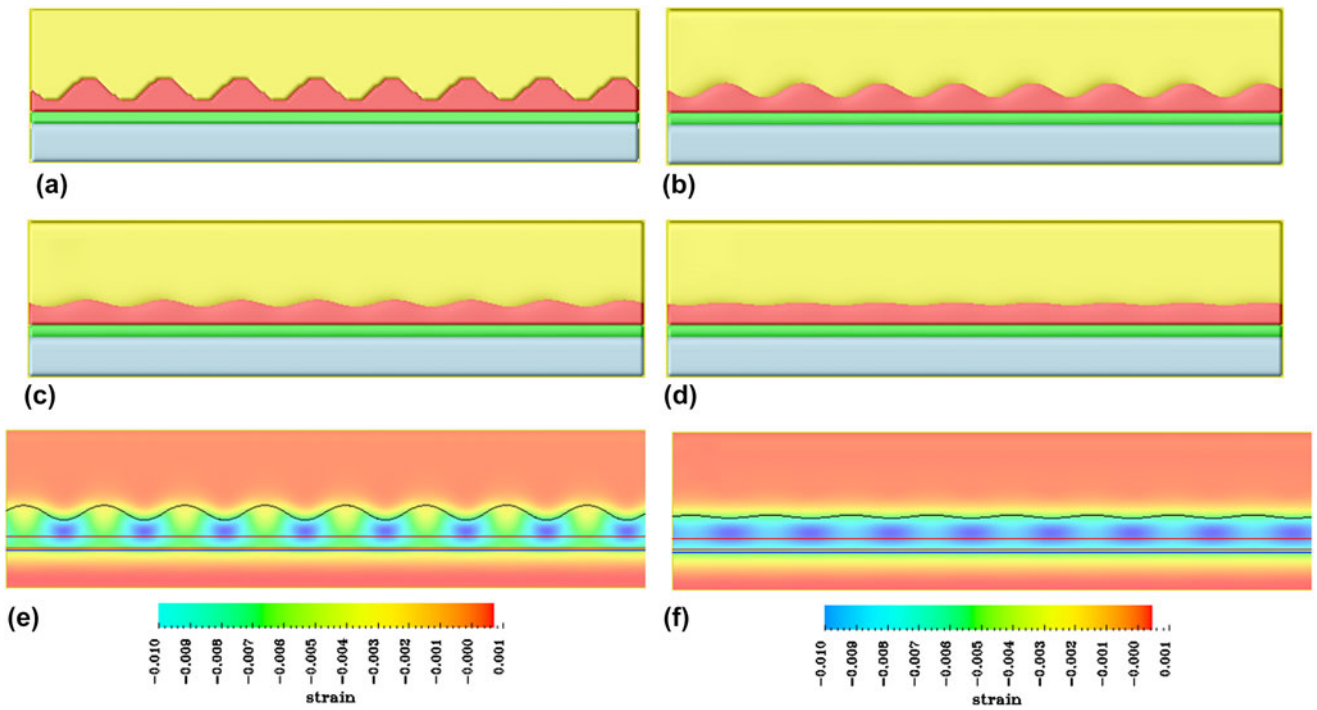

FIG. 2. The time evolution of the surface morphology: (a) initial sinusoidal wave surface, (b–d) the surface morphology after 1000, 3000, and 5000 steps evolution. (e) and (f) represents the strain distribution of 1000 steps (b) and 5000 steps (d), respectively. The black, red, and blue lines in the strain distributions represent the gas/thin film, the thin film/buffer layer, and buffer layer/substrate interfaces, respectively.

the buffer layer. Finally, as the surface morphology went smooth, we see the decrease of the surface RMS roughness.

To investigate the influence of the buffer layer thickness on the roughness of the surface morphology, the buffer layer thickness in the range from 1 to 12 nm on the substrate is used in this work. Figure 3 shows the measured RMS roughness at different buffer layer thicknesses. It can be seen that the RMS roughness sharply reduced when increasing the buffer layer thickness. One interesting feature is observed in the surface morphology with 1-nm buffer layer, as shown in the inset of Fig. 3. The surface morphologies perform nanodot structures due to the very thin buffer layer structure. The compressive strain did not relax, and the surface morphology grows and coarsens, which induced a high RMS roughness. When the thickness of the buffer layer increases further, we see a significant decrease in the RMS roughness. When the thickness exceeds 3 nm, the RMS roughness decreased below 1. An optimal thickness of 7 nm is observed in these simulation results, the surface morphology is shown in the inset of Fig. 3. Only a slight increase of the RMS roughness is observed with a high buffer layer thickness, and a similar surface morphology is received.

To understand the interplay between the buffer layers and the surface morphology through the strain relaxation with the buffer layer thickness, we performed the evolution of simulated strain distributions with several different values of buffer layer thickness. Figures 4(a)–4(d) represent the strain distribution with buffer layer thicknesses of 1, 2, 7, and 12 nm, respectively. The left column is the strain distribution after 1000 steps of evolution, and the right column is the strain distribution after 5000 steps of evolution. It is seen that the surface roughness decreases when larger buffer layer thickness is used. It is interesting to observe that the surface roughness decreases very fast when the thickness varies from 1 to 3 nm, which suggest that the surface morphology is highly sensitive to the thickness of the buffer layers. The observation of the distribution

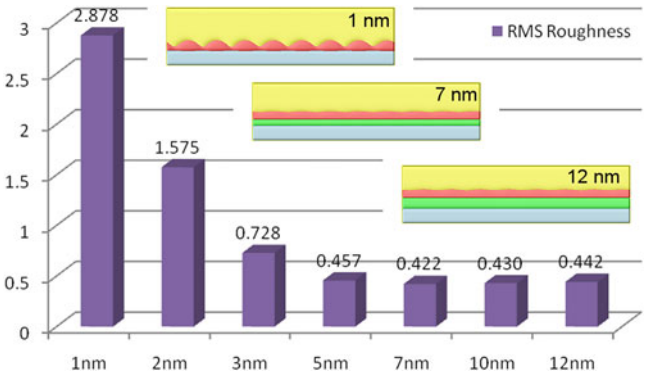

FIG. 3. The RMS roughness of the surface morphology with different buffer thicknesses varies from 1 to 12 nm. The inset morphology figures represent the buffer thickness of 1, 7, and 12 nm, respectively.

from Fig. 4(a) shows a strong compressive strain at the trough of the wave of the surface morphology. As the buffer layer thickness is rather small, the internal strain is still nonuniform after 5000 steps evolution, which introduced a high RMS roughness of the surface and a slight perpetuation of the substrate/buffer interface in the simulation. The nonuniform strain distribution led to a nanodot structure and the surface roughening process, which implies that the increased surface area results in an increase in the surface energy but in a greater reduction of the elastic energy and the total free energy of the system.[19,20] After the buffer layer thickness reaches 2 nm, a gradual change of the strain was clearly seen on the thin film/buffer layer interface under the trough of the sinusoidal wave of the surface morphology at early times, and then the strain distribution uniformity increases, which led to a sharp decrease of the surface roughness. With a further increase in the buffer layer thickness [Fig. 4(c)], the strain distribution is almost uniform and a high quality thin film is received. If a higher buffer layer thickness is assumed, such as 12 nm, a small increase in RMS roughness is obtained, which can be explained by the internal strain that needs some more time to reach the uniform state when the thickness increases. The simulation results revealed that the surface roughness of the epitaxial bilayer thin film is strongly correlated with the buffer layer thickness. The strain distribution for different buffer layer thicknesses well explained how the buffer layers work to decrease the surface roughness by strain distribution uniformity.

Based on these simulation results shown above, it was found that the buffer layer thickness was a key parameter to affect the surface morphology and the quality of the epitaxial thin film. However, a very small thickness, which is similar to the case of no buffer layers, makes the surface morphology coarsen due to the fact that the thin film relaxes its internal stress via forming the nanodot structures. As a buffer layer is added between the thin film and the substrate, internal compressive strain can be relaxed through the buffer layer structures. There exists an optimal thickness of 7 nm in the buffer structures, which is also observed in some III–V semiconductor experimental studies.[7] Similar simulation results are received by an initial random small fluctuation of surface morphology profile, which is popularly used in previous phase-field works.[21–24] With further increase in the buffer layer thickness, the high buffer layer generates a stable surface for the rest of the thin film to grow on; while the thickness of the thin film remains constant, the $In_{0.3}Ga_{0.7}As$ thin film is likely to grow on the $In_{0.15}Ga_{0.85}As$ substrate with a new lattice parameter, which may induce a slight increase of the RMS roughness. It should be noted that, in experimental, the thickness of a buffer affects the growth mode, structural and optical properties, and the density of defects of the epitaxial thin film.[6–8] Especially the defects, like point defects or dislocations, may affect the surface morphologies and its RMS roughness.

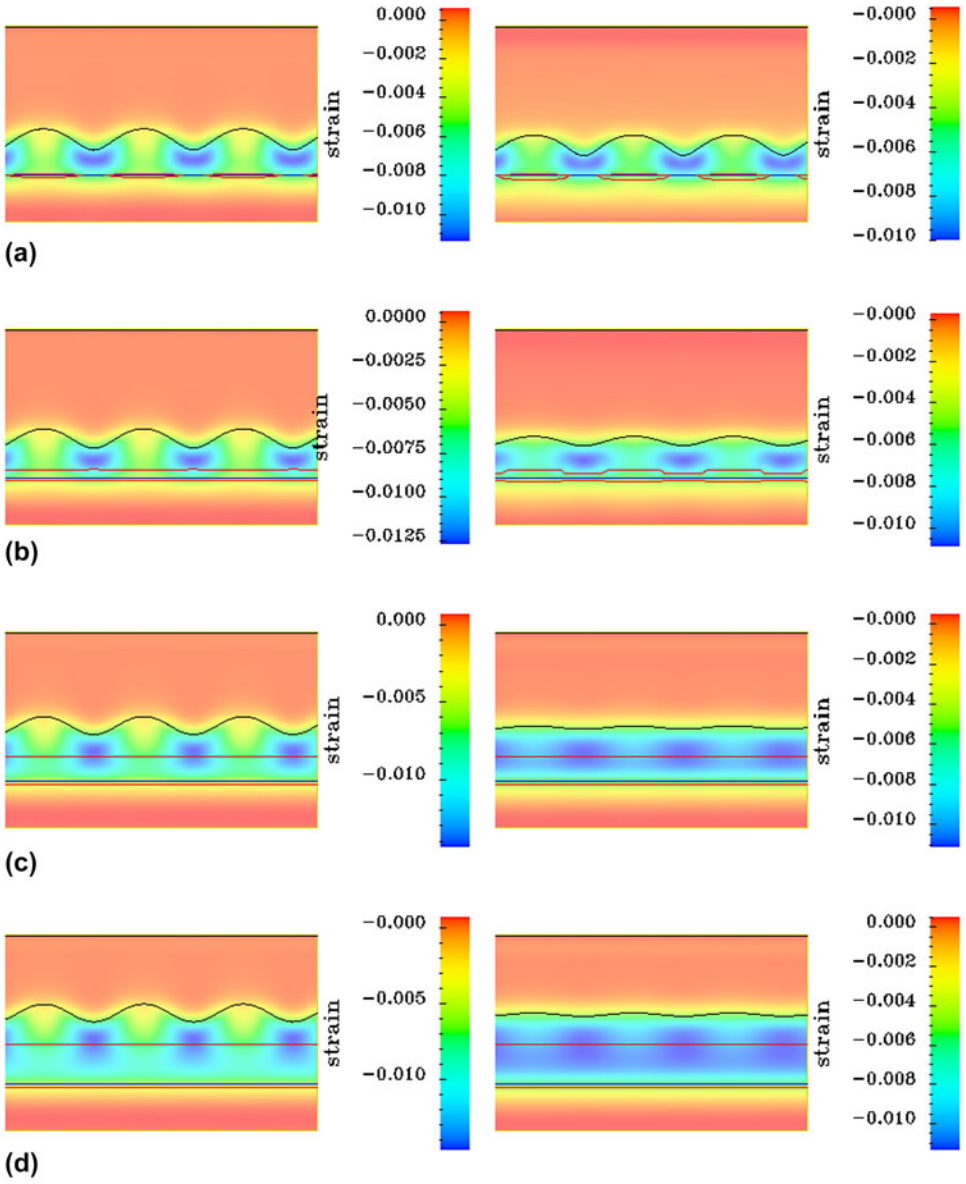

FIG. 4. (a–d) The strain distribution evolution of the GaAs/InGaAs heterostructures with a buffer layer thickness of 1, 2, 7, and 12 nm, respectively. The black, red, and blue lines represent the gas/thin film, the thin film/buffer layer, and buffer layer/substrate interfaces, respectively.

To understand the influence of the defects on the surface morphology, the phase-field model needs to be extended to include the defect mechanism both in the thin film and the buffer layers.

IV. CONCLUSION

In summary, a phase-field model is developed to simulate the $In_{0.3}Ga_{0.7}As$ thin film grown on the GaAs substrate with $In_{0.15}Ga_{0.85}As$ buffer layer structures. The evolution of the surface morphology, RMS roughness, and the strain distribution is examined in the current phase-field model. The coarsened nanodot structure is observed with a very thin buffer layer. It is found that the RMS roughness sharply reduced with an increase in the buffer layer thickness. However, the roughness slightly increases at a high buffer thickness. An optimal buffer layer thickness of 7 nm is predicted. The model with the role of defect mechanism is under development, which will be included in the future works.

ACKNOWLEDGMENTS

This work was supported by National Key Basic Research Project of China (Grant No. 973 Project), National Science Foundation of China (Contract Nos. 51002052

and 51372001), and Key Project in Science and Technology of Guangdong Province (Contract No. 2011A080801018). P. W. also would like to acknowledge funding from China Postdoctoral Science Foundation No. 2013M531840.

REFERENCES

1. R.R. King, D.C. Law, K.M. Edmondson, C.M. Fetzer, G.S. Kinsey, H. Yoon, R.A. Sherif, and N.H. Karam: 40% efficient metamorphic GaInP/GaInAs/Ge multijunction solar cells. *Appl. Phys. Lett.* **90**, 183516 (2007).
2. W. Guter, J. Schöne, S.P. Philipps, M. Steiner, G. Siefer, A. Wekkeli, E. Welser, E. Oliva, A.W. Bett, and F. Dimroth: Current-matched triple-junction solar cell reaching 41.1% conversion efficiency under concentrated sunlight. *Appl. Phys. Lett.* **94**, 223504 (2009).
3. M. Wiemer, V. Sabnis, and H. Yuen: 43.5% efficient lattice matched solar cells. *Proc. SPIE*, Vol. **8108**, 810804, High and Low Concentrator Systems for Solar Electric Applications VI (2011). doi: 10.1117/12.897769.
4. A. Luque: Will we exceed 50% efficiency in photovoltaics? *J. Appl. Phys.* **110**, 031301 (2011).
5. D.J. Dunstan: Relaxed buffer layers. *Semicond. Sci. Technol.* **6**, A76 (1991).
6. J.C. Zhang, D.G. Zhao, J.F. Wang, Y.T. Wang, J. Chen, J.P. Liu, and H. Yang: The influence of AlN buffer layer thickness on the properties of GaN epilayer. *J. Cryst. Growth* **268**, 24 (2004).
7. X.L. Wang, D.G. Zhao, X.Y. Li, H.M. Gong, H. Yang, and J.W. Liang: The effects of LT AlN buffer thickness on the properties of high Al composition AlGaN epilayers. *Mater. Lett.* **60**, 3693 (2006).
8. W.J. Luo, X.L. Wang, L.C. Guo, H.L. Xiao, C.M. Wang, J.X. Ran, J.P. Li, and J.M. Li: Influence of AlN buffer layer thickness on the properties of GaN epilayer on Si(1 1 1) by MOCVD. *Microelectron. J.* **39** 1710 (2008).
9. S. Nakamura: GaN growth using GaN buffer layer. *J. Appl. Phys.* **30**, L1705 (1991).
10. L. Gonzalez, J.M. García, R. García, F. Briones, J. Martínez-Pastor, and C. Ballesteros: Influence of buffer-layer surface morphology on the self-organized growth of InAs on InP(001) nanostructures. *Appl. Phys. Lett.* **76**, 1104 (2000).
11. E.C. Piquette, P.M. Bridger, R.A. Beach, and T.C. McGill: Effect of buffer layer and III/V ratio on the surface morphology of Gan grown by MBE. In *MRS Proceedings*, Vol. **537**, 1998; p. G3.77. doi:10.1557/PROC-537–G3.77.
12. R.J. Asaro and W.A. Tiller: Interface morphology development during stress corrosion cracking: Part I. Via surface diffusion. *Metall. Trans.* **3**, 1789 (1972).
13. M.A. Grinfeld: Instability of the separation boundry between a nonhydrostatically stressed elastic body and a melt. *Sov. Phys. Dokl.* **31**, 831 (1986).
14. D.J. Srolovitz: On the stability of surfaces of stressed solids. *Acta Metall.* **37**, 621 (1989).
15. H. Gao: Some general properties of stress-driven surface evolution in a heteroepitaxial thin film structure. *J. Mech. Phys. Solids* **42**, 741 (1994).
16. J. Tersoff and F.K. LeGoues: Competing relaxation mechanisms in strained layers. *Phys. Rev. Lett.* **72**, 3570 (1994).
17. R. Krishnamurthy and D.J. Srolovitz: Film/substrate interface stability in thin films. *J. Appl. Phys.* **99**, 043504 (2006).
18. G.H. Lu and F. Liu: Towards quantitative understanding of formation and stability of Ge hut islands on Si(001). *Phys. Rev. Lett.* **94**, 176103 (2005).
19. F. Liu: Self-assembly of three-dimensional metal islands: Nonstrained versus strained islands. *Phys. Rev. Lett.* **89**, 246105 (2002).
20. H. Wang, Y. Zhang, and F. Liu: Enhanced growth instability of strained film on wavy substrate. *J. Appl. Phys.* **104**, 054301 (2008).
21. H. Hu, H.J. Gao, and F. Liu: Theory of directed nucleation of strained islands on patterned substrates. *Phys. Rev. Lett.* **101**, 216102 (2008).
22. Y.U. Wang, Y.M. Jin, and A.G. Khachaturyan: Phase field microelasticity modeling of surface instability of heteroepitaxial thin films. *Acta. Mater.* **52**, 81 (2004).
23. D.J. Seol, S.Y. Hu, Z.K. Liu, L.Q. Chen, S.G. Kim, and K.H. Oh: Phase-field modeling of stress-induced surface instabilities in heteroepitaxial thin films. *J. Appl. Phys.* **98**, 044910 (2005).
24. Y. Ni, L.H. He, and A.K. Soh: Three-dimensional phase field simulation for surface roughening of heteroepitaxial films with elastic anisotropy. *J. Cryst. Growth* **284**, 281 (2005).
25. T. Takaki, T. Hirouchi, and Y. Tomita: Phase-field study of interface energy effect on quantum dot morphology. *J. Cryst. Growth* **310**, 2248 (2008).
26. S.R. Kurtz, D. Myers, and J.M. Olson: Projected performance of three- and four-junction devices using GaAs and GaInP. In *Photovoltaic Specialists Conference*, 1997; Conference Record of the Twenty-Sixth IEEE, 1997; pp. 875–878. doi: 10.1109/PVSC.1997.654226.
27. D.J. Friedman, J.F. Geisz, A.G. Norman, M.W. Wanlass, and S.R. Kurtz: 0.7-eV GaInAs junction for a GaInP/GaAs/GaInAs(1eV)/GaInAs(0.7eV) four-junction solar cell. *4th World Conference on Photovoltaic Energy Conversion*, 2006; p. 598–602. doi: 10.1109/WCPEC.2006.279527.
28. J.F. Geisz, S.R. Kurtz, M.W. Wanlass, J.S. Ward, A. Duda, D.J. Friedman, J.M. Olson, W.E. McMahon, T.E. Moriarty, J.T. Kiehl, M.J. Romero, A.G. Norman, and K.M. Jone: Inverted GaInP/(In)GaAs/InGaAs triple-junction solar cells with low-stress metamorphic bottom junctions. In *Photovoltaic Specialists Conference San Diego, California May 11–16, 2008*, 33rd IEEE; 2008; pp. 1–5. doi: 10.1109/PVSC.2008.4922452.
29. S.M. Sze: *Physics of Semiconductor Devices*, 2nd ed. (Wiley, New York, 1981).
30. M.R. Pillai, S-S. Kim, S.T. Ho, and S.A. Barnett: Growth of $In_xGa_{1-x}As/GaAs$ heterostructures using Bi as a surfactant. *J. Vac. Sci. Technol., B* **18**, 1232 (2000).
31. J.W. Matthews and A.E. Blakeslee: Defects in epitaxial multilayers: III. Preparation of almost perfect multilayers. *J. Cryst. Growth* **32**, 265 (1976).
32. J.M. Millunchick and S.A. Barnett: Suppression of strain relaxation and roughening of InGaAs on GaAs using ion-assisted molecular beam epitaxy. *Appl. Phys. Lett.* **65**, 1136 (1994).
33. A.G. Khachaturyan: *Theory of Structural Transformations in Solids* (Wiley, New York, 1983).
34. L.Q. Chen and J. Shen: Applications of semi-implicit Fourier-spectral method to phase field equations. *Comput. Phys. Commun.* **108**, 147 (1998).
35. I.V. Kurilo and S.K. Guba: Misfit dislocations and stress in $In_{1-x}Ga_xAs/GaAs$ heterostructures. *Inorg. Mater.* **47**, 819 (2011).
36. T. Anan, K. Nishi, and S. Sugou: Critical layer thickness on (111)B-oriented InGaAs/GaAs heteroepitaxy. *Appl. Phys. Lett.* **60**, 3159 (1992).
37. S.L. Chuang: *Physics of Optoelectronic Devices* (Wiley, New York, 1995).
38. S.O. Mariager, S.L. Lauridsen, A. Dohn, N. Bovet, C.B. Sørensen, C.M. Schleputz, P.R. Willmott, and R. Feidenhans'l: High-resolution three-dimensional reciprocal-space mapping of InAs nanowires. *J. Appl. Cryst.* **42** 369, (2009).
39. M. Pelliccione and T.M. Lu: *Evolution of Thin Film Morphology Modeling and Simulations* (Springer, New York, 2007).

40. J.W. Matthews and A.E. Blakeslee: Defects in epitaxial multilayers: I. Misfit dislocations. *J. Cryst. Growth* **27**, 118 (1974).
41. D.C. Bertolet, J-K. Hsu, F. Agahi, and K.M. Lau: Critical thickness of GaAs/InGaAs and AlGaAs/GaAsP strained quantum wells grown by organometallic chemical vapor deposition. *J. Electron. Mater.* **19**, 967 (1990).
42. M. Krieger, H. Sigg, N. Herres, K. Bachem, and K. Kohler: Elastic constants and Poisson ratio in the system AlAs–GaAs. *Appl. Phys. Lett.* **66**, 682 (1994).
43. W.E. Hoke, T.D. Kennedy, and A. Torabi: Simultaneous determination of Poisson ratio, bulk lattice constant, and composition of ternary compounds $In_{0.3}Ga_{0.7}As$, $In_{0.3}Al_{0.7}As$, $In_{0.7}Ga_{0.3}P$, and $In_{0.7}Al_{0.3}P$. *Appl. Phys. Lett.* **79**, 4160 (2001).
44. P.J. Orders and B.F. Usher: Determination of critical layer thickness in $In_xGa_{1-x}As$/GaAs heterostructures by x-ray diffraction. *Appl. Phys. Lett.* **50**, 980 (1987).
45. A. Jasik, J. Sass, K. Mazur, and M. Wesolowski: Investigation of strained InGaAs layers on GaAs substrate. *Opt. Appl.* **37**, 237 (2007).
46. X. Zhang, O. Briot, B. Gil, and R. Aulombard: Critical layer thickness in MOCVD grown InGaAs/GaAs strained quantum wells. *Mater. Sci. Eng., B* **35**, 184 (1995).